scientific reports

Check for updates

OPEN

Sequence of events that led to the South Lhonak lake outburst flood in Sikkim, India

Litan Kumar Mohanty[1,2]✉, Prateek Gantayat[3]✉, Ankur Dixit[4], Manik Das Adhikari[5], Rahul Biswas[6] & Vivek Kumar Singh[7]

On October 4, 2023, a proglacial lake named the South Lhonak lake was the source of a catastrophic Glacier Lake Outburst Flood (GLOF) in the Teesta river basin area, resulting in 24 fatalities and leaving over 70 persons missing. The GLOF also destroyed 13 bridges and a major hydropower plant in the Chungthang region. Over 60,000 individuals in four districts of Sikkim were impacted by this GLOF event. This study examines the factors that led to the GLOF event. Our study shows that the cause of this GLOF was initiated by a landslide, that dumped a substantial amount (~ 38.31 million m^3) of debris into the South Lhonak Lake. Furthermore, the glacier that was connected to the lake, lost a big chunk of ice mass (~ 7 million m^3) due to calving. The combination of these two processes led to the collapse of the left lateral moraine that consequently generated flood waves which breached the terminal moraine dam of the lake. We recommend monitoring land subsidence and calving events for large proglacial lakes to prevent the disastrous consequences of such GLOFs in the future.

Proglacial lakes form through glacier/ice meltwater accumulation in the topographic depressions that get exposed due to the glacier's retreat[1]. Ice-contact, large proglacial lakes in many cases, extend across the glacier's width thereby leading to ice-melt through to the glacier's bed as well as rapid glacier retreat due to calving near the terminus (e.g[2]. The Himalaya is the home to 1116 proglacial lakes as of 2020[3]. These lakes are often found in rugged and remote terrain that renders them extremely vulnerable to natural hazards such as Glacier Lake Outburst Floods (GLOFs). GLOFs are natural hazards that release enormous amounts of water within a short period due to failure of the lake's moraine dam failure or overtopping of the lake's water. A few most common triggers of GLOFs are landslide, avalanche, cloudburst, and accelerated melting rate of glaciers (e.g., [4,5]. Out of 703 Himalayan GLOF events recorded since 1833, 28 were triggered by heavy precipitation, followed by temperature rise (15), ice avalanches (28), rock falls (2), ice calving (1), upstream floods (1), and landslides (1)[6]. Outside the polar regions, only 2% of GLOFs have been said to be triggered by earthquakes[7]. The spatial and elevation-wise distribution of GLOF events in the Himalaya is shown in Fig. 1.

The risk of GLOFs is exacerbated due to the growing number of glacial lakes (both in number and volume), which, upon reaching their full capacity (or even prior to that), could lead to catastrophic flooding. Since the beginning of the nineteenth century, 165 moraine-dam GLOFs have been recorded, with 55 of them occurring in the Hindu Kush Himalaya (HKH)[4]. Additionally, historical data show that since 1560, 296 GLOF events occurred from 109 lakes[8], 45% of them were recorded in the Eastern Himalaya and their occurance has been attributed to the failure of moraine dam[8]. Alarmingly, 62% of the globally exposed population live in the Himalayan region[9], highlighting the region's significant vulnerability. The Eastern Himalayan region, in particular, is facing double the risk compared to its adjacent regions[8]. Increasing GLOF occurrences are observed alongside an increasing rate of glacial lake formations in recent times. Since 1990, the number, area, and volume of glacial lakes has grown by 53%, 51%, and 48% globally[9]. However, the increase in glacial lakes area in the Himalayas is found to be 26%, 17%, 76%, and 30% during the 1990–2020, 1990–2018, 1990–2018, and 1990–2010, respectively[10–12,15]. 48.3% increase in the proglacial lake area occurred between 1990 and 2020 with > 15.5% change occurring over the period 2010 and 2020[3]. Notably, the highest concentration of these expanding lakes is found to be in the Eastern Himalaya[11].

The Eastern Himalaya also witnessed the highest number of GLOF occurrences in the High Mountain Asia (HMA)[5]. This region experienced several catastrophic GLOFs, such as the Cirenmaco outburst in 1981 in the

[1]Wadia Institute of Himalayan Geology, Dehradun, India. [2]Central Ground Water Board, Bhubaneswar, India. [3]Institute of Science and Technology Austria, Klosterneuburg, Austria. [4]Cornell University, Ithaca, USA. [5]Gangneung-Wonju National University, Gangneung, Korea. [6]CSIR-National Geophysical Research Institute, Hyderabad, India. [7]Center for Environmental Sensing and Modelling, Singapore MIT Alliance for Research and Technology, Singapore, Singapore. ✉email: mohanty.litan.geo@gmail.com; gantayat.prateek@ymail.com

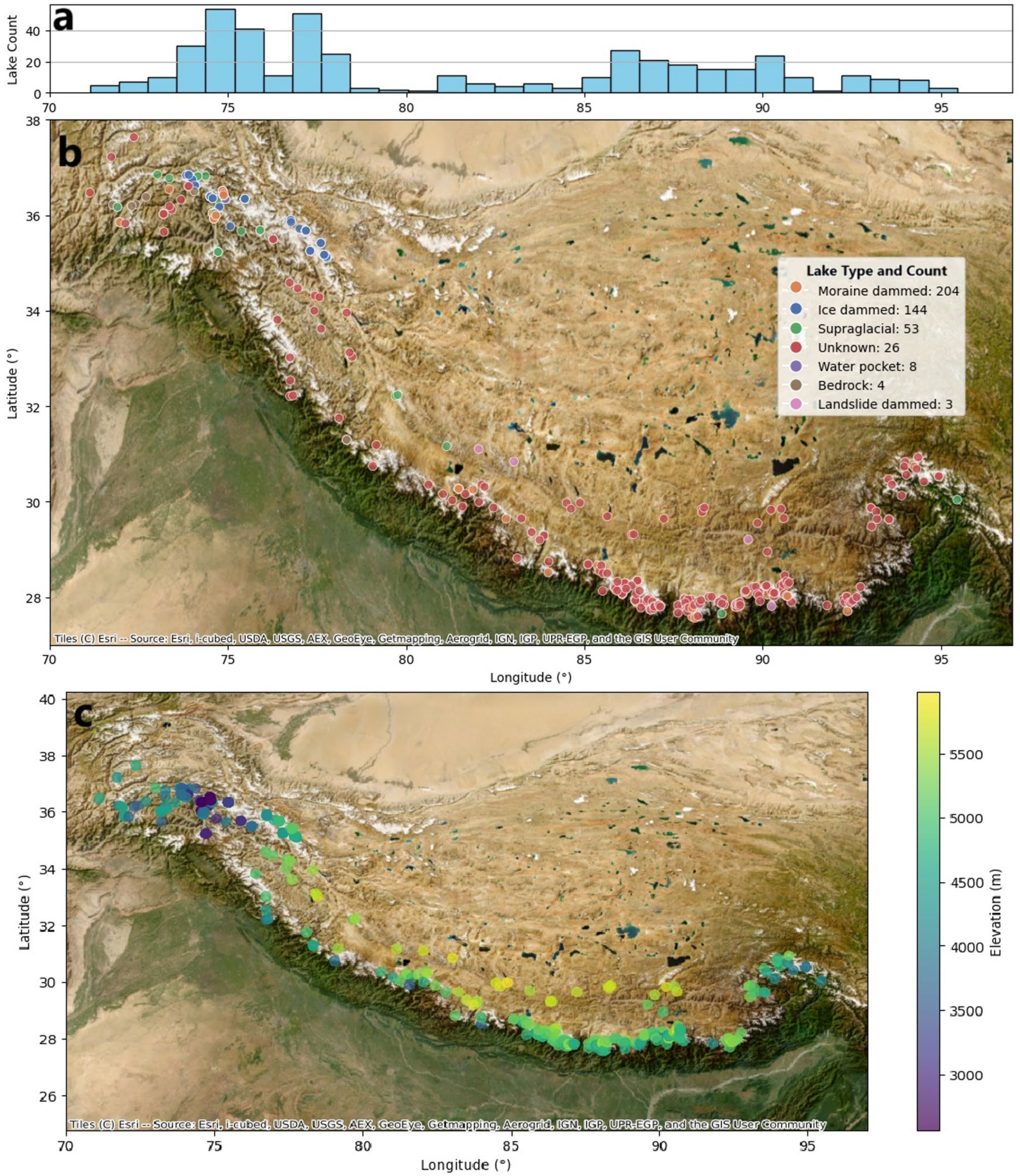

Fig. 1. The spatial distribution of the frequency of the occurrence of the GLOFs is shown in (**a**). (**b**) The coloured dots show the location and the different types of lakes (e.g., ice-dammed, supraglacial, moraine-dammed, landslide-dammed) that underwent GLOF in the Himalaya. (**c**) Elevation-wise spatial distribution of the GLOF events in the Himalaya. The figure was produced using ArcMap 10.1 (https://www.arcgis.com/).

Sun Koshi River basin[12], the Dig Tsho incident in 1985[13,14] and the Tam Pokhari event in 1998 in the Dudh Koshi river basin[15]. Reference[3] showed that around 6353 km^2 of land is susceptible to future GLOF events, which poses a risk to > 55,000 buildings, >100 hydropower projects, ~ 200 km^2 of cropland, ~ 5000 km of highways, and > 4000 bridges.

The South Lhonak lake is located in the Eastern part of the Himalayas. On early hours of October 4th, 2023, the lake became the source of one of the most devastating GLOF in recent times. The flood waves originated due to the lake's dam breach, which increased the water level in the downstream regions by 15–20 feet[16], affecting more than 25,000 individuals, destroying 1200 residences and sweeping away 13 bridges, including the Chungthang dam (located ~ 60 km from the South Lhonak lake).

Recent literature on the event (e.g., [17] suspected heavy rainfall, excessive glacier calving and mass movements from the sidewalls to be the major triggers, leading to breaking of the lake's moraine dam, resulting in the GLOF. But these studies predominantly concentrated the downstream impacts of the GLOF. Consequently, there is still a significant gap in understanding the role of triggers that caused the GLOF in terms of the sequence of events and/or the possibility of those triggers acting in a compound manner.

Due to complex dynamics behind the triggering mechanism, studying isolated events with their potential triggers could inform a meaningful insight for necessary steps to be taken to prevent such hazards or reduce the impact to the least. In this study, we attempt to study the event (3rd October 2023 in South Lhonak lake) to infer the following.

1. What is the comprehensive list of triggers that led to the South Lhonak GLOF?
2. Which one among the probable triggers played the most dominant role?

Study area

Our study area includes the South Lhonak lake and the valley walls surrounding the lake (Fig. 2). It is located in the northern region of the Teesta Basin, within the Indian state of Sikkim in the Eastern Himalaya at an

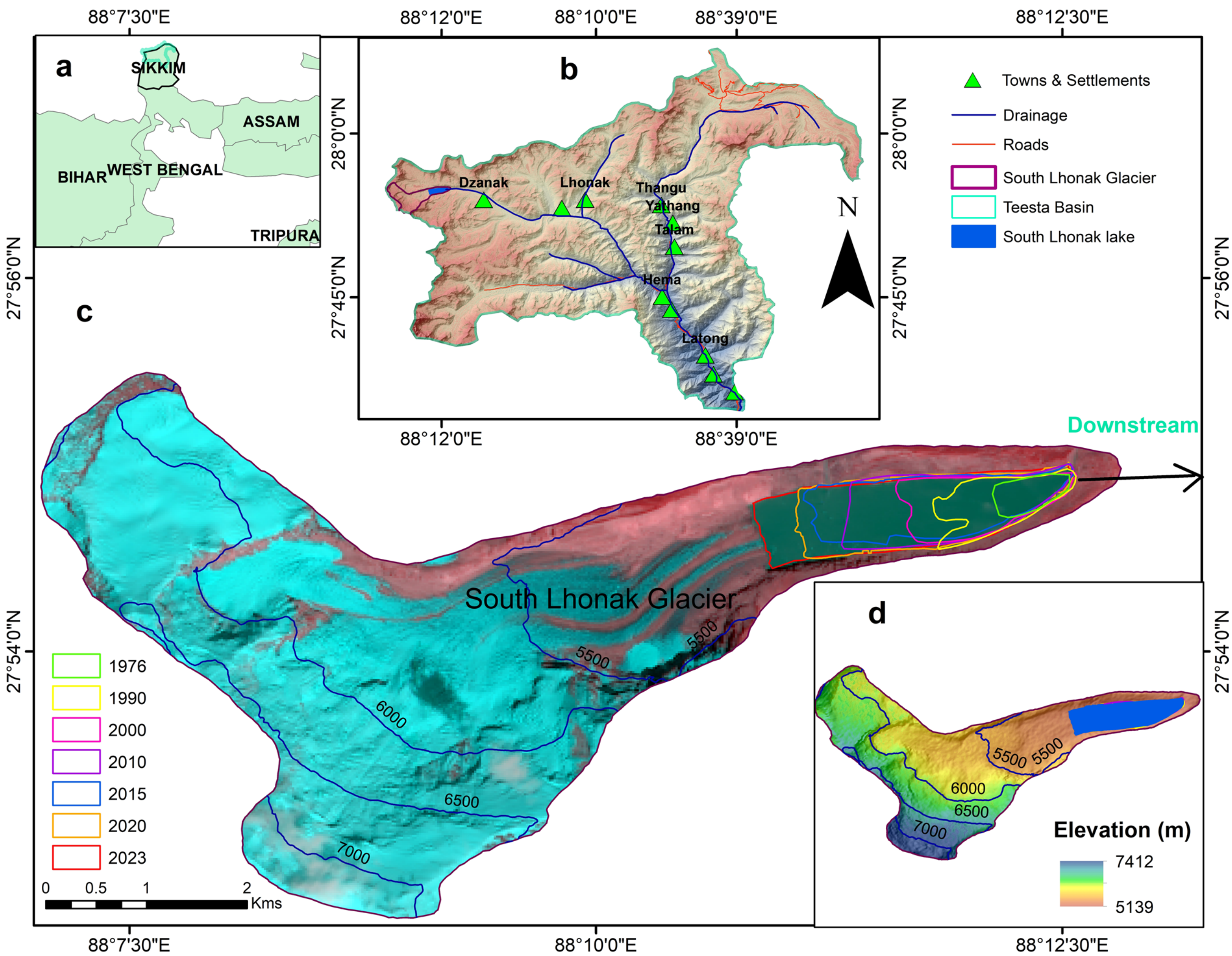

Fig. 2. (**a**) Location of the South Lhonak lake in the state of Sikkim in India. (**b**) The solid green line represents the boundary of the Teesta basin. The green triangles represent the location of various towns and settlements located along the flood-path of the stream originating from the South Lhonak lake. (**c**) The thin blue lines represent the surface elevation contours of the glacier. The coloured lines (i.e., shown on the lake) represent the time series of the lake boundaries between the period 1976 and 2023. (**d**) Surface elevation of the South Lhonak glacier varies between ~ 7400 m and 5150 m. The figure was produced using ArcMap 10.1 (https://www.arcgis.com/).

altitude of 5400 m[18]. The lake is connected to the South Lhonak glacier and is formed when glacier-melt water accumulated in the exposed bed overdeepening due to the retreat of the glacier.

At one end, the lake is surrounded by the calving front of the South Lhonak glacier that is at an elevation of ~ 5200 m a.s.l. and at the other end, the lake is surrounded by a frontal moraine that is 18 m high (i.e., with respect to the lake's surface, prior to the GLOF) and has a height to width ratio of 0.031[19]. It had an aerial extent of ~ 1.35 km^2 in 2016[19]. In situ bathymetric survey conducted in 2016 estimated the lake volume to be ~ 66 million m^3 with a maximum and mean depth of 131 m and 67 m, respectively[19].

The lake was growing with a consistent rate of 0.03 km^2a^{-1} in its aerial extent, 0.04 km^2a^{-1} in its length between 1976 and 2016[19]. The lake is susceptible to GLOF, as it is located in a region that is susceptible to avalanches and landslides (e.g.,[20]). Past studies (e.g.,[21–24]) have reported this lake to be extremely vulnerable to GLOFs due to heightened calving at the glacier's front and avalanches, with the latter being the most probable trigger[25].

Methodology and data used

We individually analyse the following probable geomorphologic and climatic triggers that might have caused the GLOF.

i. landslide from the surrounding lake walls;
ii. calving from the connected glacier;
iii. rainfall in the region.

Breach height in the lake's moraine dam

We estimate the breach height that is necessary for the lake water to overtop the height of the moraine dam. Breach height refers to the vertical height of the breach, measured from the dam's crest down to the lowest point of the breach. It is typically calculated as the difference between the water surface elevation before the breach and the lowest elevation of the breach after the dam's failure.

To estimate breach height, we first use Sentinel-2 imagery (~ 10 m resolution) to delineate the lake boundaries. We then estimate the lake volume using Bayesian Calibration based proglacial lake estimation model BEGLAV[26]. BEGLAV is a novel, numerical model based on the assumption that along a proglacial lake's centerline, the lake's cross-sectional geometry is trapezoidal in nature. The model then uses Bayesian inference to estimate the cross-sectional geometry at grid points (i.e., placed along the lake's centerline) placed 50 m apart by minimising the difference between modelled and measured lake surface widths along those grid points. Consequently, the model produces lake volume with extremely robust bounds on the uncertainty.

We then estimate the Peak Flood Discharge (PFD) using the scaling relationship using Froehlich equation:

$$\mathrm{Qp} = 0.607 * (\mathrm{A_w})^{0.295} * (\mathrm{h_w})^{1.24} \tag{1}$$

where: Qp is the peak discharge (m^3/s). A_w is the surface area of the reservoir at the time of failure (m^2).

h_w is the height of the water above the breach bottom at the time of failure (m). These equations assume that the dam is made of earth or rockfill materials, and the breach develops as a result of overtopping or piping.

Based on the magnitude of pre-GLOF lake volume and the associated PFD, we estimate the failure time (T_f) using Froechlich's equation:

$$\mathrm{T_f} = 0.00254 * (\mathrm{V})^{0.53} * (\mathrm{H_b})^{-0.9} \tag{2}$$

where H_b is the breach height which is defined as the minimum height that the flood waves from the lake should attain in order to overtop the moraine dam of the lake. We estimated the H_b as 40 m by DEM differencing of the 30 m spatial resolution, Advanced Spaceborne Thermal Emission and Reflection Radiometer (ASTER) acquired on 14/05/2024 (http://scihub.copernicus.eu/dhus) and the 8 m spatial resolution, HMA DEM acquired during the period 2002–2016 (https://nsidc.org/data/hma_dem8m_mos/versions/1) (Figs. S2 and S11; Supplementary). It must be noted that prior to differencing, the ASTER DEM was resampled to a spatial resolution of 8 m from 30 m. We used the approach developed by Nuth and Kääb[27] for differencing the two DEMs.

Landslide and debris volume estimation

Delineation of landslide zone and surface displacement

To delineate the landslide area and to estimate the surface displacement, we use the Band-5 of Sentinel-2 imagery. We opted for Band-5 due to the high emissivity of soil/ debris in this spectral band. We use two images corresponding to the dates 14-02-2023 (pre-GLOF) and 09-10-2023 (post-GLOF) for estimating displacement near south Lhonak lake using Cosi-Corr software package. Cosi-Corr has been used in various studies to identify the velocity or deformation of earth's surface due to earthquake, landslide, glacier movement and dune migration by wind[28]. It uses auto-correlation of two orthorectified satellite images (i.e., one prior and the other after the landslide event) to detect sub-pixel ground deformations/motion[29].

Estimation of volume of the landslide that entered the lake

Having delineated the landslide zone, we then use a scaling relationship by Jaboyedoff et al.[30] to estimate the volume of landslide material that slumped into the lake just prior to the GLOF:

$$\mathrm{V} = \mathrm{k} * \mathrm{A_s}^{\alpha} \tag{3}$$

where, V is the volume of material displaced, K is the constant, A_s is the surface area from which the landslide occurred and α is an exponent.

We set α as 1.45 and k as 0.074, as those values have been derived for large landslides (e.g.,[31]). Large landslides are those where the A_s is constrained in the range [2 m^2 and 10^9 m^2] (e.g.,[31]). Those values are derived from the Worldwide Catalouge of Landslides[31], after excluding the submarine landslides.

Estimation of volume from calving from the glacier onto the lake

High spatial resolution (10 m) Sentinel 2 data is used to estimate the morphological changes near the lake and glacier snout, for both pre- and post-event. The calving area is estimated through visual inspection while the thickness of the glacier calving zone is estimated using the ice thickness estimation model proposed by Gantayat et al.[32]. The model assumes Shallow Ice Approximation (e.g.,[33]) and estimates ice thickness from surface velocities and surface slope as shown in Eq. (4).

$$h_i = 4\sqrt{\frac{1.5U_{si}}{A^3(C\rho g\sin\alpha_m)^3}} \tag{4}$$

where, U_{si} is the Surface Velocity field, n is the Glen's flow law exponent (we used as 3), A is the reep or flow rate factor (depends on temperature, fabric, grain size, and impurity content), is inferred to be 3.24×10^{-24} $Pa^{-3}s^{-1}$ from previous works done on alpine glaciers, C is correction factor, assumed to be 0.8 in our analyses (e.g.,[32]), ρ = ice-density (900 kg m^{-3}), g = Acceleration due to gravity (9.8 m s^{-2}) and α_m = Mean surface slope along the flow-line.

Estimation of precipitation during GLOF event

We examined precipitation using the IMERG-L dataset from October 2nd to October 5th, 2023. It provides near-real time precipitation with a spatial resolution of 0.1 degrees and a temporal resolution of 30 min. IMERG-L utilizes both forward and backward propagation strategies to update precipitation estimates using rain gauge data. Additionally, WRF experiments are conducted at convection-permitting scale to investigate precipitation and constituent atmospheric conditions in the GLOF affected region. WRF is run from 01 Oct 2023 to 08 Oct 2023, at 4 km resolution, provided with Indian Monsoon Data Assimilation and Analysis (IMDAA) initial and boundary conditions. Noah-MP is used to represent land surface models and constituent options for physical parameterization schemes are adopted from Dixit et al.[34] (see Table S1 for details).

Estimation of ground subsidence from SAR interferometry

Sixty-four Sentinel-1 images are acquired from the European Space Agency (ESA) Copernicus Open Access Hub (http://scihub.copernicus.eu/dhus) in Single Look Complex (SLC) format, between October 8, 2017 and January 14, 2021 to produce a time series of maps showing subsidence and upliftment in the valley walls surrounding the lake and the glacier (e.g., Fig. S1; Supplementary). We used the Shuttle Radar Topography Mission (SRTM) Digital Elevation Model (DEM) for geocoding and topographic correction of the subsidence maps.

Further, PS-InSAR technique proposed by Ferretti et al.[35] is used to monitor land-subsidence at millimeter precision[36]. This technique has the capability to detect points or targets (i.e., the Permanent Scatterers (PS)) that remain unchanged over the time period. For PS-InSAR analysis, we co-register Single Look Complex (SLC) images of the same area to a single master configuration, which is typically selected based on perpendicular and temporal baseline to maximize interferometric coherence (e.g.,[37]). Thereafter, interferograms are generated using multi-temporal SAR images (i.e., during the period 2017 till 2021). Finally, the orbital data and the external SRTM DEM are used to remove the influence of Earth's curvature and the topographic component of the interferometric phase, respectively.

For the sake of brevity, all the datasets that have been used in this study have been listed in Table S3 (Supplementary text).

Results

Volume and projected peak flood discharge of the lake prior to the GLOF

The pre-GLOF volume of the South Lhonak lake was estimated to be 131.9 ± 33.8 million m^3. The corresponding peak flood discharge estimated using Froelich's equation is ~ 12,399 m^3/s. From the difference map that was created by differencing the ASTER DEM and the HIMAT DEM, the erosion of the lake's moraine dam was estimated to be ~ 40 m (Fig. S2; Supplementary) which was also assumed to be the breach height (H_b). Therefore, the failure time was estimated to be ~ 1.84 h (Fig. S2; Supplementary).

Estimation of moraine displacement in the landslide zone

The displacement of the moraine in the landslide zone is estimated to be ~ 30–100 m (Fig. 3b). The surface displacement map, generated from Sentinel-2 imagery, clearly demonstrates substantial downstream movement to the snout. These movements could be related to the displacement of lake water, moraine, and debris caused by the flood. The left lateral moraine shows a noticeable shift or wearing away due to the wave generated in the lake by the landslide and calving. In addition, we discovered significant subsidence in the vicinity of the landslide area, measuring average of ~ 32 mm/year (i.e., with a range of displacement ~ 10–54 mm/year, estimated using SARPROZ software package (https://www.sarproz.com) (Fig. 3a and Fig. S1 (Supplementary)). Higher vertical subsidence is found near the lake outlet along with the decline in the lake surface level (Fig. 3a).

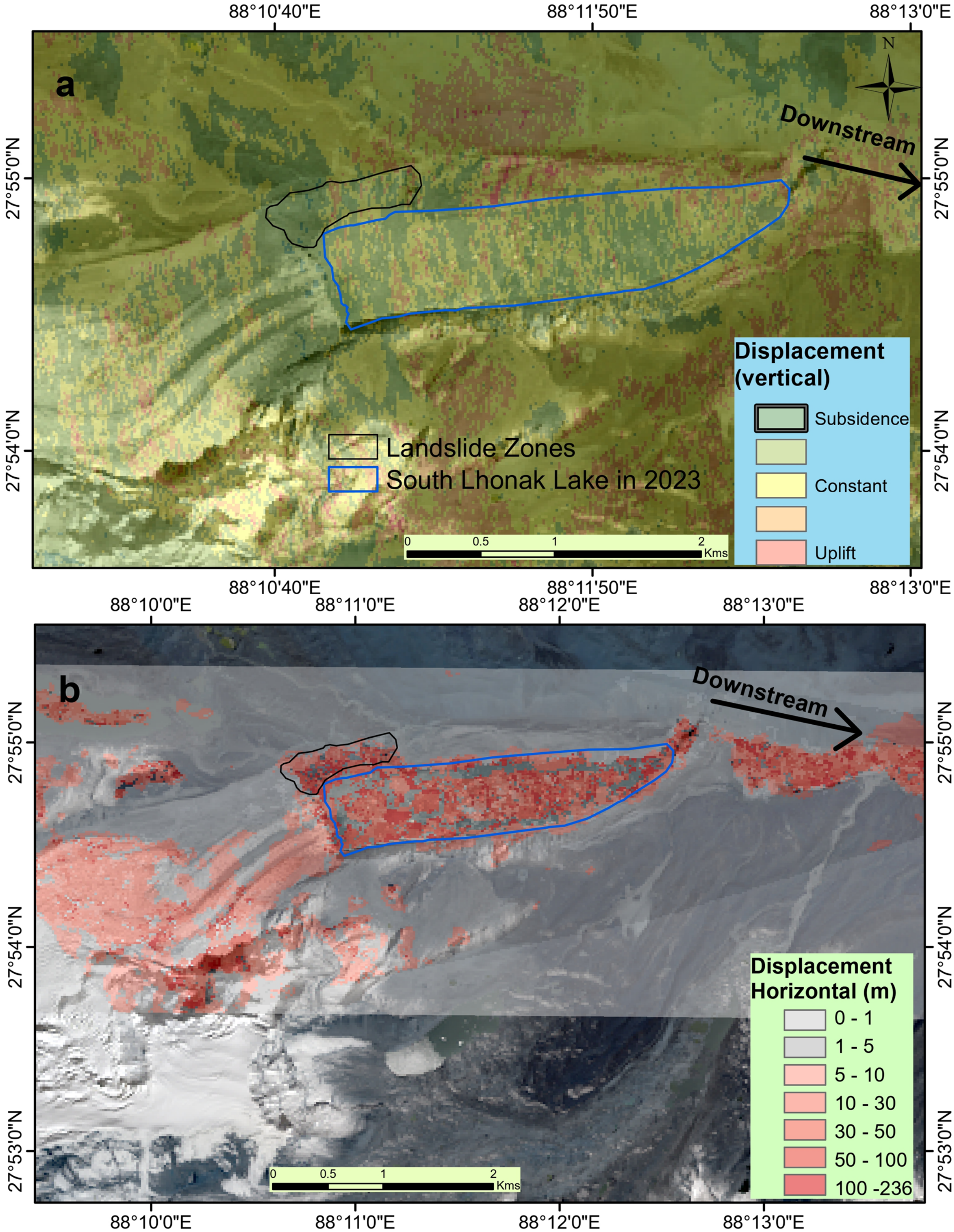

Fig. 3. (**a**) Sentinel-1 imagery derived vertical subsidence map of the South Lhonak lake region as measured between 25-09-2023 and 07-10-2023. (**b**) Horizontal displacement map of the South Lhonak lake region (i.e., for the period 14-09-2023 and 09-10-2023) as derived from Sentinel-2 imagery. The timestamp of the base map is 09-10-2023. In both (**a**) and (**b**) the black-coloured-outlined polygon on the left lateral moraine represents the region from where the landslide originated on 4th October 2023 (i.e., on the day of the GLOF). The maps were produced using ArcMap 10.1 (https://www.arcgis.com/).

Volume of the debris and ice deposited into the lake due to landslide and glacier-calving

Based on visual inspection and displacement maps (from Sentinel-2 imagery), the landslide affected area is estimated to be ~0.23 million m^2. Consequently, using Eq. (3) the volume of landslide is found to be ~38.31 million m^3.

The mean ice thickness at the calving front of the connected glacier is estimated to be ~124 m, using Eq. (4). The corresponding calving volume was estimated to be ~7.11 million m^3 (Fig. 4a). Assuming the entire mass displacement related to landslide and calving got deposited into the lake, the volume of water displaced from the lake is equal to the volume of mass (i.e., from calving and landslide) entering the lake i.e., ~45.42 million m^3. We believe this generated intense pressure on the dam wall, resulting in its failure and rapid release of the stored water.

Discussions

Most likely sequence of events leading to the GLOF

The South Lhonak glacier retreated by more than 100 m, between February-September of 2023, leading to an accelerated input of glacier ice into the lake through frontal calving (Fig. 5a). This rapid retreat likely left behind dead ice along the left lateral moraine of the glacier (Fig. 5a), further weakening the structure. Similar instances of glacier destabilization due to calving have been observed in the past, such as in the Gangotri glacier system, where the retreat of the Meru glacier destabilized the lateral moraine of the Gangotri glacier, triggering a large debris flow in 2017 (Ref.[38]; see Fig. S10, Supplementary).

In the South Lhonak region, precipitation between 27th September and 3rd October 2023 contributed to liquefaction along the left lateral moraine (~2.09 mm on 27th September, 33.96 mm on 29th September, ~51.21 mm on 30th September, ~1.20 mm on 1st October, ~9.75 mm on 2nd October, and ~97.64 mm on 3rd October). Notably, precipitation peaked on 3rd October with 97.64 mm, along with significant precipitation on 29th and 30th September. This precipitation along with runoff from snowmelt/rainfall seeping through moraine led to further instability (marked within the black polygon in Fig. 5a). Additionally, two water streams (S1 and S2, Fig. 7a) supplied water to the lake, originating from glacier X and the North Lhonak glacier. These streams carved through the left lateral moraine at two critical points namely i and ii (Fig. S12, Supplementary), adding further pressure to the already weakened structure.

Moreover, the glacier's left lateral moraine was already classified as susceptible to landslides due to its steep slope along the transects x–x′, y–y′ and z–z′ that was estimated to be 43%, 36%, and 48%, respectively (Fig. S12; Supplementary). This natural vulnerability was further exacerbated by the glacier retreat, liquefaction from precipitation events, and the increased meltwater discharge from the two streams into the lake.

On 4th October 2023, the combination of these factors led to a landslide along the glacier's front, triggering further calving of ice from the glacier. This landslide is measured as an average length and width of ~0.15 km and ~0.34 km, respectively (Fig. 5a,b,d) from the South Lhonak glacier's front (located near to the landslide zone). The corresponding volume of the landslide material that got deposited into the lake was estimated to be ~38.31 million m^3 (i.e., from Eq. 3). The volume of the ice mass that calved into the lake following the landslide was estimated to be ~7 million m^3. The deposition of ice (~7 million m^3) and landslide debris (~38 million m^3) into the South Lhonak lake produced impulsive flood waves that exerted immense pressure on the terminal moraine (Figs. 1 and 5c), ultimately causing the dam wall to break and resulting in a Glacial Lake Outburst Flood (GLOF). Our analyses suggest that the addition of ice and landslide debris led to the displacement of ~45 million m^3 of the lake' waters which is comparable to 50 million m^3 derived by the study conducted by Sattar et al.[40].

Our analysis concludes that the rapid glacier retreat, together with liquefaction-induced landslides and increased meltwater input, played a critical role in destabilizing the left lateral moraine. The subsequent landslide-triggered calving and the resulting flood waves acted in unison, leading to the GLOF.

Impact of earthquake and time of lake outburst

We selected the USGS-estimated intensity maps with peak ground acceleration (PGA) for the M5.7 Nepal earthquake and the M4.9 Goalpara earthquake due to the proximity of the epicenter to our study region i.e., the South Lhonak lake area (https://www.usgs.gov/programs/earthquake-hazards/earthquakes). Data namely the location of the epicenter, time of occurrence of the earthquake and the corresponding Modified Mercalli Intensity (MMI) and PGA are extracted and processed to overlay the earthquake intensities and contours on a map of the study area. We focused on identifying intensity zones and assessing the corresponding potential impacts of the earthquake in regions where weak to light shaking was observed. A comparison of the shaking effects of the different earthquakes, suggested that the Goalpara earthquake likely had a more significant impact as compared to the Dipyal Earthquake (in Nepal) (Fig. 6), due to its proximity of its location and time of occurrence to the lake and the GLOF event, respectively (Fig. S10 and Table S2; Supplementary). A list of earthquakes in the region near the South Lhonak lake area has been shown in Table S2 (Supplementary). Except for Golpara earthquake, the other earthquakes occurred in the vicinity of Dipyal (20–60 km) and had intensity lower than the one shown in Fig. 6a and so they have not been shown in Fig. 6. However, as evident from the intensity map (Fig. 6), even the shaking effects of the Goalpara earthquake were either weak or very light. So we suspect that the earthquake had minimal effect on the South Lhonak lake GLOF.

These maps were produced by ShakeMaps, developed by the USGS, which represent ground shaking intensity and PGA contours following an earthquake. However, ShakeMaps have limitations, as they provide generalized estimates and assume uniform ground conditions, neglecting the effect of local geological variations.

The South Lhonak Lake lies within the "weak shaking" zone (Instrumental Intensity II) during the M 4.9 Goalpara earthquake (2 October 2023, 12:45 p.m.), as shown in Fig. 6. According to USGS ShakeMap scaling[41], this corresponds to PGA values below 0.297%g (≈0.003 g). The impact of the M 5.7 Nepal earthquake was even smaller due to its larger epicentral distance. Thus, even for the nearest event, seismic shaking at the lake

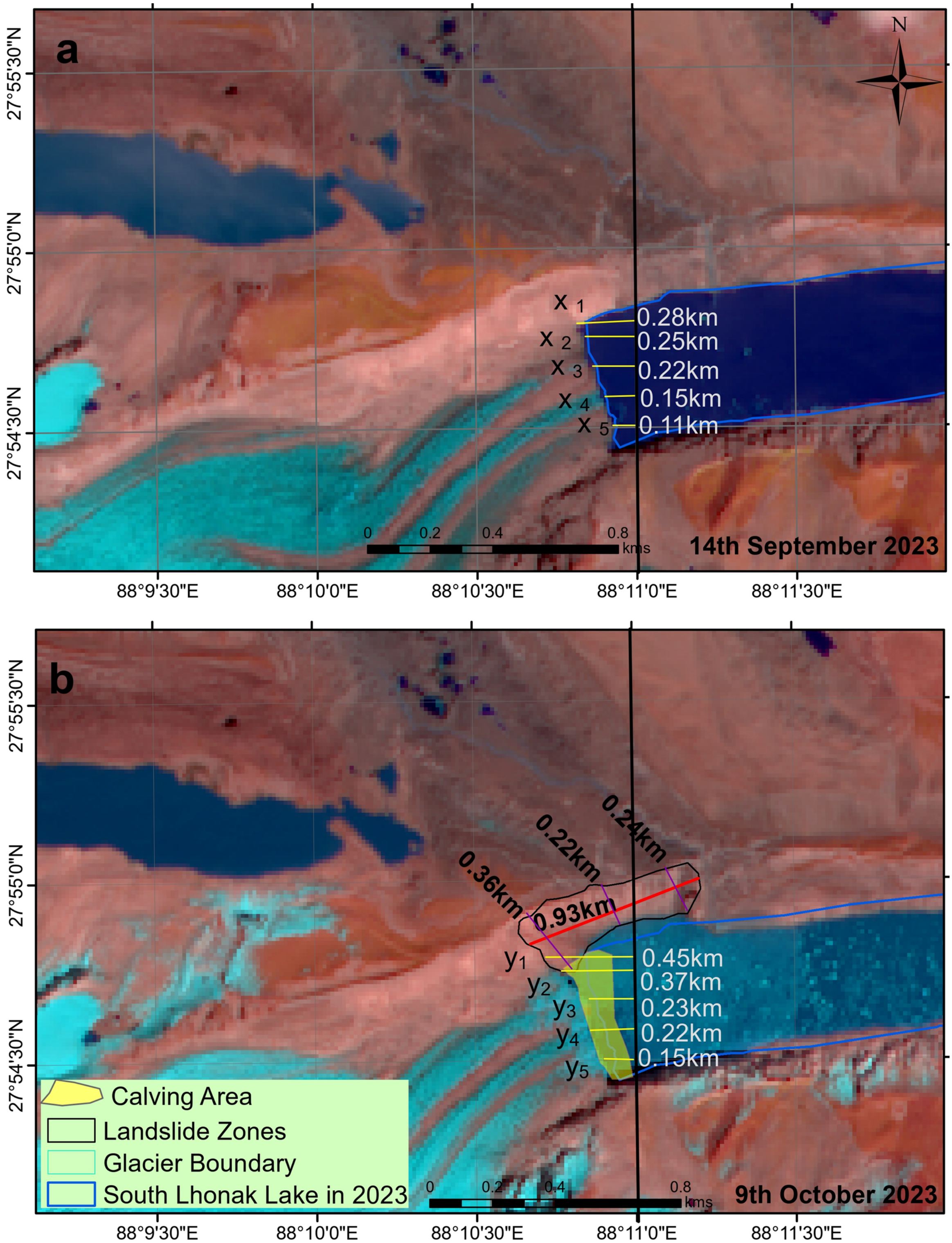

Fig. 4. Landslide and Calving width and length estimation using Sentinel 2 data. (**a**) is the pre-event image. The distance of the glacier's front is measured from the black vertical line shown in the image. Timestamp of the basemap is 14-09-2023. The calving width of the glacier front is estimated to be ~ 0.7 km. (**b**) The shaded yellow region shows the area of the glacier front that calved into the lake. The hollow black polygon represents the region on the glacier's left lateral moraine that deposited landslides into the lake. Timestamp of the basemap imagery is 09-10-2023. The figure was produced using ArcMap 10.1 (https://www.arcgis.com/).

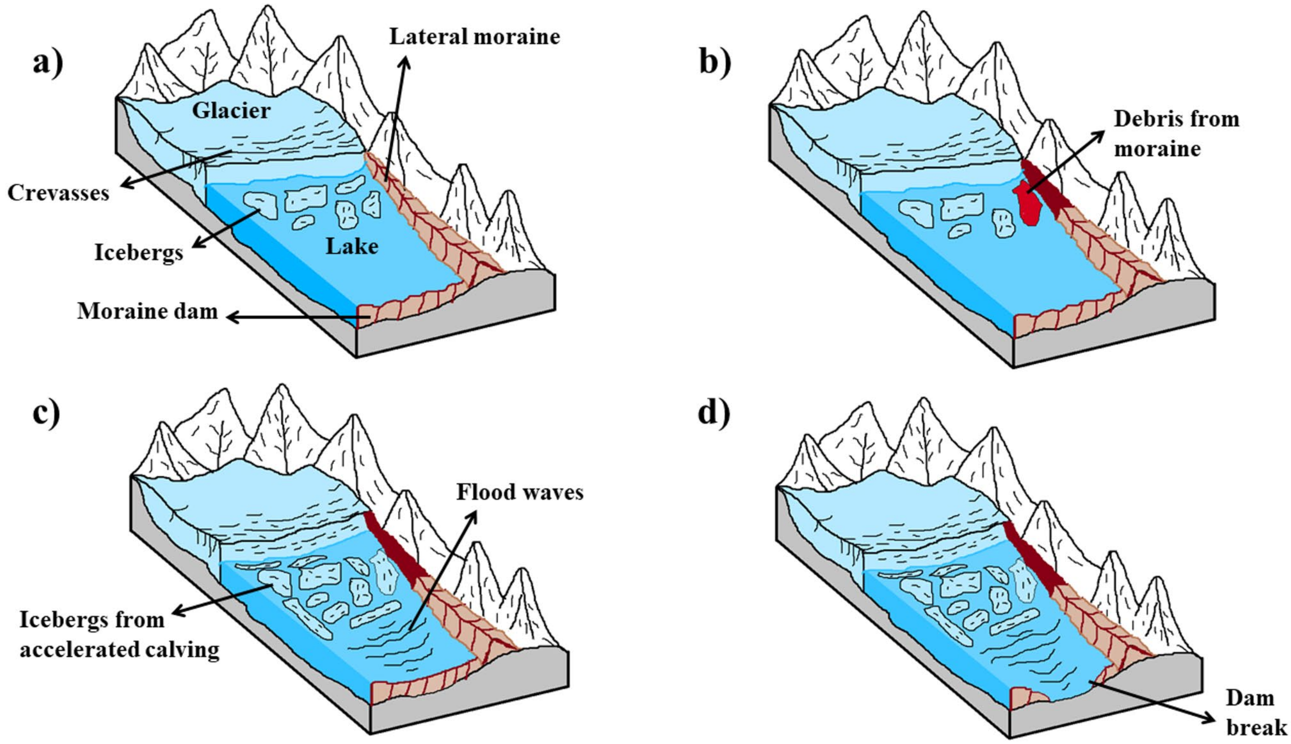

Fig. 5. Schematic of the sequence of the events that led to the GLOF at the South Lhonak lake. (**a**) Calving event from the South Lhonak lake's connected glacier (i.e., the South Lhonak glacier) between February 2023 and September 2023 that led to the glacier's retreat by > 100 m. (**b**) The rapid retreat (i.e., > 100 m) completely destabilised the left lateral moraine of the lake-glacier system. The debris from the landslide zone that entered the lake has been shown in reddish-brown colour. The landslide zone is shown in dark brown colour. (**c**) The landslide event led to more calving from the South Lhonak glacier that produced flood waves (shown as thin black lines on the lake surface). (**d**) The waves subsequently broke the moraine dam and this led to the GLOF. The figure was produced using MS-paint (https://www.microsoft.com/).

was negligible and well below thresholds associated with hydrodynamic disturbance or glacial lake outburst initiation, confirming that earthquake-induced triggering can be ruled out as a causal factor.

Why heavy precipitation is unlikely to be a major trigger for the GLOF event?

There was an initial supposition that cloudburst had a role in overflowing the lake causing a dam-break wave on the lake's lateral moraine. However, we do not find any cloudburst during this event in the North Sikkim region where the lake is located. Though, a forecast bulletin by IMD released on 1 October 2023 predicted widespread rainfall over Sikkim between 2 and 4 October 2023.

Additionally, satellite precipitation from IMERG-L also reconciles with our findings (Fig. S9; Supplementary), and shows that the south Sikkim (and north-east India) received a significant precipitation (i.e., < 10 mm and 20–80 mm on 2nd and 3rd October, 2023, respectively) but north Sikkim remained mostly dry over this period.

We show atmospheric conditions and moisture transport from WRF simulations in supplementary Figs. S4–S7. We find a low-pressure system intensifying until 5th october over East and North-East India, causing excessive moisture transport. The system intensified mostly over Jharkhand, West Bengal region and moved towards east affecting the West Bengal and southern part of Sikkim. North Sikkim remained unaffected and did not see much precipitation.

Lack of evidence of heavy precipitation over the lake-region before or during the event is convincing to outrule precipitation being attributed to one of the potential active triggers for the lake outbreach. However, a fast-melting South Lhonak glacier, receded by ~ 400 m in almost a decade (from 2008 to 2019, Ref.[42]), caused a rapid growth in lake volume and made it one of the most vulnerable lakes in the region.

Uncertainty analyses

Due to the paucity of in-situ measured glacier surface velocities, we relied on estimating the potential uncertainty that is often associated with velocity images estimated via COSI-Corr. The potential uncertainty associated with COSI-Corr derived surface velocities is often believed to be 0.1–0.3 times the input image's spatial resolution, which translates into ground velocity error depending on pixel size and time interval (e.g.,[29]) as:

$$Uncertainty = r * \frac{\sigma_{offset}}{\Delta t} \tag{5}$$

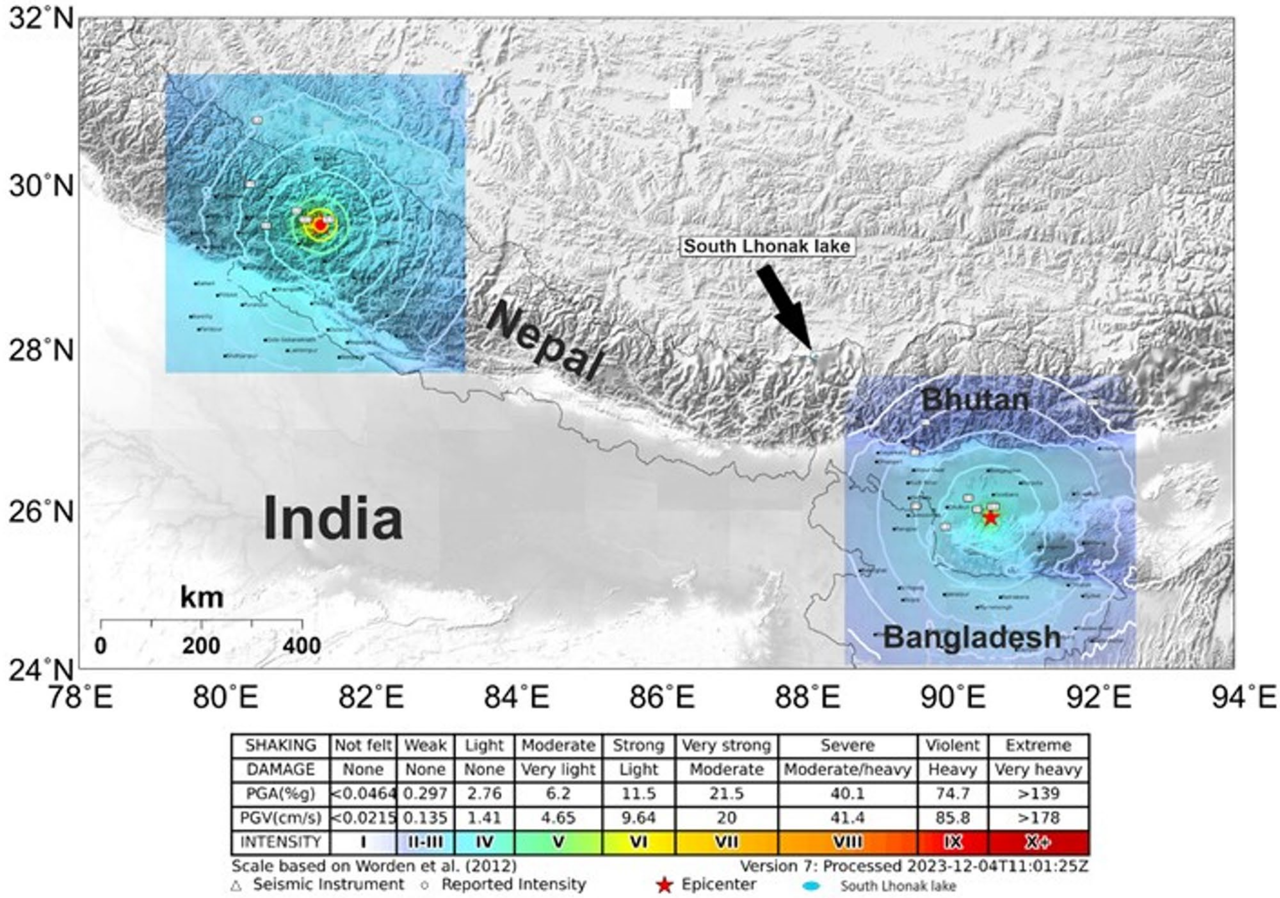

Fig. 6. Epicenter of great earthquakes around the GLOF's source (i.e., the South Lhonak lake). The distance between the South Lhonak lake and the earthquakes is mentioned in Table S2. The contours and colour around the Nepal and Goalpara earthquakes represent the PGA value and intensity, respectively. The figure was produced using ArcMap 10.1 (https://www.arcgis.com/).

where, r is the pixel size which is 10 m as we used a pair of Sentinel-2 images, σ_{offset} has a value of 0.1–0.3 and Δt is the time difference between the date of acquisition of the image which is 25 days in this study. Therefore, we assume the uncertainty in glacier surface velocity to be in the range of 0.04 and 0.12 m/day respectively. Similar to glacier surface velocities, we estimated the displacement of the lateral moraine (i.e., which resulted in the landslide) using the same set of Sentinel-2 imagery. Based on Eq. (5), the potential uncertainty in displacement is same as that of velocity.

Due to the unavailability of in-situ measured estimates of surface subsidence, we again had to rely on published sources of potential uncertainty that was esimated for Sentinel-1 imagery derived surface subsidence maps landslides occurring in the Himalayan region which is ~ 5–10 mm/year (e.g., [43]).

The rainfall pattern over our study region was inferred from IMERG dataset. Monthly values from the dataset was found to have a correlation of ~ 0.8 with that observed in the Nepalese Himalaya (e.g., [44]). In the same region, IMERGE precipitation data has been proved to successfully detect precipitation and non-precipitation days with an accuracy of > 80% (e.g., [44]).

In order to estimate the uncertainty in delineating the landslide zone, we followed the approach of Mohanty and Maiti (2021). As per the Mohanty and Maity (2021), the overall uncertainty in mapped polygonal features is estimated in terms of uncertainties associated with their outlines (e_outline) and areas (e_area). This uncertainty (i.e., e_outline and e_area) was determined by summing the half of spatial resolution of image used for feature mapping and the co-registration error (e_corr) according to Eq. (6):

$$\mathrm{e\_outline} = 1/2\,(\mathrm{spatialreolution}) + \mathrm{e\_corr}$$

The e_outline for in our case varied between 7.5 m and 15 m for different years. The e_corr in the Sentinel 2 and LISS IV imagery in Rugged mountains/glaciers: can increase to 1–2 pixels (10–20 m and 6–18 m), respectively especially with snow/ice cover, where contrast is low for tie-points. The e_area, e_outline and the polygon perimeter (l) are related as:

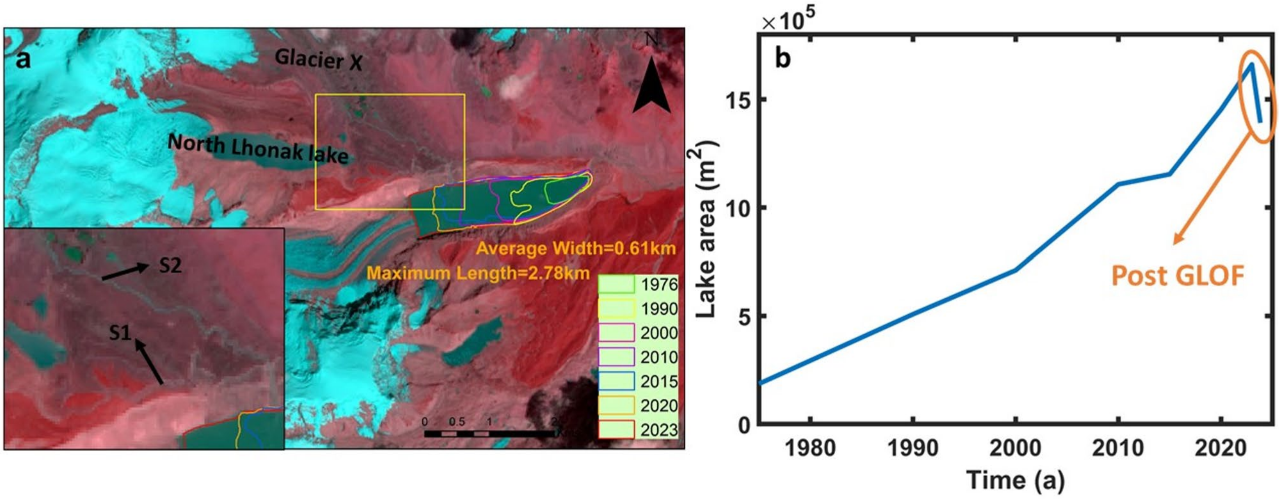

Fig. 7. In fig. (**a**,**b**) the graph shows the evolution of the lake area (in m^2). In (**a**) the evolution of the lake-area before the GLOF is shown. The meltwater channels that originate from Glacier X and the North Lhonak lake have been shown in the inset and have been labelled as S1 and S2 respectively. (**b**) shows decline in lake area in the orange color post GLOF event. The figure was produced using ArcMap 10.1 (https://www.arcgis.com/) and Matlab 2015 (https://www.mathworks.com/).

$$e\_area = \sqrt{((e\_outline)^2 * l)} \tag{6}$$

Based on Eq. (6), the e_area was estimated to be in the range 367–733 m.

Recommendations for detecting future GLOFs in the Himalayan proglacial lakes

Based on our analyses, we propose the following long-term monitoring strategies:

Monitoring of ground subsidence

We found that the ice-free region surrounding the South Lhonak lake consistently underwent a subsidence between 2017 and 2021 at an average rate of ~ 22 mm/a. The subsidence could be due to the melting of underlying ice-cores present underneath the moraines in those regions. Our analyses showed significant subsidence between 2017 and 2021, from the left lateral moraine of the lake (i.e., the region from where the landslide occurred into the lake) (see Fig. 3 and supplementary Figure S1 for details).

We therefore recommend regular monitoring of the land subsidence of the regions surrounding large proglacial lakes (like the South Lhonak lake) in the Himalaya.

Monitoring rate of expansion of lake area

Using Sentinel 2 and LISS IV satellite imagery ((https://bhoonidhi.nrsc.gov.in/) and https://dataspace.copernicus.eu/), we estimated the increase in the lake area between 1975 and 2023 by ~ 0.27 km^2 (i.e., by ~ 8 times between that time period) (Fig. 7). The growth rate appears to be monotonically increasing with a rate of ~ 16.49%$year^{-1}$. The observed, high rate of lake growth is potentially due to the many significant calving events (at least four) between 2022 and 2023, from the South Lhonak glacier (Fig. S11; Supplementary).

Therefore, we think it is essential to monitor the rate of calving events in the case of large proglacial lakes that are still joined to their respective connected glaciers.

Monitoring the status of past flood monitoring measures that were undertaken at the South Lhonak lake

In 2016, the Department of Science and Technology, under the Government of Sikkim, conducted a field visit to South Lhonak lake. The purpose of the expedition was to measure lake-bathymetry and to build an early warning system to detect GLOFs. Bathymetric studies carried out by Sharma et al.[19] in 2016, estimated the deepest point in the lake and the lake volume to be ~ 130 m, and ~ 65 million m^3. An AWS (Automatic Weather Station) was installed at the south Lhonak lake that became inoperative in 2016 as a result of a collision with an iceberg that got calved from the South Lhonak glacier.

Furthermore, a total of 140 pipelines were employed to artificially siphon the discharge of lake water in this particular area. The discharge recorded near the outlet was around 4.5 cubic meters per second (160 cubic feet per second) according to the DST Sikkim report 2016 (http://icestupa.org/news/slug-rb4s71). The flow rate from a single pipeline is roughly 50 L per second, resulting in a total flow rate of 150–180 L per second across three sets of pipelines in 2016 (DST, Sikkim Report). But, the anticipated reduction of the lake's water level (i.e., by ~ 2 m) at the end of the winter season was unsuccessful due to an unexpectedly rapid melting event (https://dstsikkim.gov.in/mech/South%20Lhonak%20Lake%20mitigation%20expedition.pdf).

In the future we recommend regular monitoring of such installed infrastructure at all the critical proglacial lakes in order to mitigate the effects of any future GLOF event.

Conclusion

In this study, we present the sequence of events that led to the outburst of the South Lhonak lake on 4th October, 2023. Our analyses showed that the lateral moraine located along the left-side of the glacier's calving front was experiencing subsidence at an average rate of ~ 22 mm/year since 2019.

Prior to the GLOF event (i.e., before 4th October, 2023), the rapid upstream expansion of the lake by > 100 m (i.e., along the centerline of the connected glacier) that happened within one year, due to four major calving events, left dead-ice beneath the left-lateral moraine that rendered it unstable. This unstability of the left-lateral moraine was further enhanced due to the sudden increase in discharge of two meltwater channels that cut though it and empty their respective waters into the South Lhonak lake. These meltwater channels historically have carried runoff from the upstream-located glacier X and a proglacial lake (i.e., the North Lhonak lake) to the South Lhonak lake. The increase in the discharge of these meltwater channels was due to excessive surface melting from the glacier X in the early days of October.

In addition to the above, the unstability of the left moraine was also enhanced by the seepage of the snow-melt-derived water into it. This snowmelt was the result of the medium precipitation events that occurred between 29th September, 2023 and 3rd October, 2023.

The above events, combinedly led to the failure of the left-lateral moraine located near the connection between the South Lhonak lake and its connecting glacier on 4th October, 2023 leading to the addition of ~ 38.31 million m^3 of moraine debris into the lake. This addition of debris into the lake led to further calving from the South Lhonak glacier that added ~ 7 million m^3 of ice into the lake. The addition of ice (i.e., due to calving from the South Lhonak glacier) and debris (i.e., from the landslidefrom the left-lateral moraine) into the South Lhonak lake led to displacement of ~ 45 million m^3 of lake water that produced flood waves which eventually lead to the GLOF on 4th October, 2023.

In order to mitigate the effects of future GLOF events originating from Himalayan proglacial lakes, we recommend regular monitoring of the rate of lake growth and the rate of subsidence of the lateral moraines present along the lake's as well as along the connected glacier's margins.

Data availability

Data can be accessed upon request by contacting the corresponding author via email.

Received: 27 October 2024; Accepted: 8 January 2026
Published online: 24 March 2026

References

1. Wang, H. et al. Can the GPM IMERG hourly products replicate the variation in precipitation during the wet season over the Sichuan Basin, china? *Earth Space Sci.* **7** (5), e2020EA001090. https://doi.org/10.1029/2020EA001090 (2020).
2. Sakai, A., Nishimura, K., Kadota, T. & Takeuchi, N. Onset of calving at supraglacial lakes on debris-covered glaciers of the Nepal himalaya. *J. Glaciol.* **55** (193), 909–917. https://doi.org/10.3189/002214309790152555 (2009).
3. Zhang, G. et al. Underestimated mass loss from lake-terminating glaciers in the greater Himalaya. *Nat. Geosci.* **16**(4), 333–338 (2023).
4. Harrison, S. et al. Climate change and the global pattern of moraine-dammed glacial lake outburst floods. *Cryosphere*. **12**(4), 1195–1209 (2018).
5. Veh, G., Korup, O., von Specht, S., Roessner, S. & Walz, A. Unchanged frequency of moraine-dammed glacial lake outburst floods in the himalaya. *Nat. Clim. Change*. **9** (5), 379–383 (2019).
6. Shrestha, F. et al. A comprehensive and version-controlled database of glacial lake outburst floods in high mountain Asia. *Earth Syst. Sci. Data*. **15** (9), 3941–3961 (2023).
7. Wood, J. L. et al. Shaking up assumptions: earthquakes have rarely triggered Andean glacier lake outburst floods. *Geophys. Res. Lett.* **51**(7), e2023GL105578 (2024).
8. Zheng, G. et al. The 2020 glacial lake outburst flood at Jinwuco, tibet: causes, impacts, and implications for hazard and risk assessment. *Cryosphere* **15** (7), 3159–3180 (2021).
9. Taylor, C., Robinson, T. R., Dunning, S., Rachel Carr, J. & Westoby, M. Glacial lake outburst floods threaten millions globally. *Nat. Commun.* **14** (1), 487 (2023).
10. Zhang, G., Yao, T., Xie, H., Wang, W. & Yang, W. An inventory of glacial lakes in the third pole region and their changes in response to global warming. *Glob. Planet Change*. **131**, 148–157 (2015).
11. Mohanty, L., Pateswary, V., Maiti, S. & Mohanty, D. D. Future prediction of existing glacial lake's size in the himalaya by Markov model and glacial surface topography. *All Earth*. **35** (1), 329–343 (2023b).
12. Wang, W. et al. Integrated hazard assessment of cirenmaco glacial lake in Zhangzangbo valley, central Himalayas. *Geomorphology* **306**, 292–305 (2018).
13. Richardson, S. D. & Reynolds, J. M. An overview of glacial hazards in the Himalayas. *Quatern. Int.* **65**, 31–47 (2000).
14. Bajracharya, B., Shrestha, A. B. & Rajbhandari, L. Glacial lake outburst floods in the Sagarmatha region. *Mt. Res. Dev.* **27** (4), 336–344 (2007).
15. Shugar, D. H. et al. Rapid worldwide growth of glacial lakes since 1990. *Nat. Clim. Change*. **10**(10), 939–945 (2020).
16. Zhang, G. et al. Characteristics and changes of glacial lakes and outburst floods. *Nat. Rev. Earth Environ.* 1–16 (2024).
17. Saha, S. et al. Identification of the multiple causes of recent series of landslides and related damage by extreme rainfall and GLOF in Sikkim Himalaya, India, during October 2023. *Landslides*. 1–17 (2024).
18. Raj, K. B. G., Remya, S. N. & Kumar, K. V. Remote sensing-based hazard assessment of glacial lakes in Sikkim himalaya. *Curr. Sci.* 359–364 (2013).
19. Sharma, R. K., Pradhan, P., Sharma, N. P. & Shrestha, D. G. Remote sensing and in situ-based assessment of rapidly growing South Lhonak glacial lake in Eastern Himalaya, India. *Nat. Hazards*. **93**, 393–409 (2018).
20. Guha, S. & Tiwari, R. K. Analysis of differential glacier behaviour in Sikkim Himalayas in view of changing climate. *Geocarto Int.* **37** (27), 16020–16042 (2022).

21. Sattar, A., Goswami, A. & Kulkarni, A. V. Hydrodynamic moraine-breach modeling and outburst flood routing-A hazard assessment of the South Lhonak lake, Sikkim. *Sci. Total Environ.* **668**, 362–378 (2019).
22. Mohanty, L., Maiti, S. & Dixit, A. Spatio-temporal assessment of regional scale evolution and distribution of glacial lakes in himalaya. *Front. Earth Sci.* **10**, 1038777 (2023a).
23. Mohanty, L. K. & Maiti, S. Regional morphodynamics of supraglacial lakes in the everest himalaya. *Sci. Total Environ.* **751**, 141586 (2021a).
24. Mohanty, L. & Maiti, S. Probability of glacial lake outburst flooding in the Himalaya. *Resour. Environ. Sustain.* **5**, 100031 (2021).
25. Hazra, P. & Krishna, A. P. AHP Based Assessment of Glof Susceptibility of South Lhonak Glacial Lake, Sikkim Himalaya, India. In *2021 IEEE International Geoscience and Remote Sensing Symposium IGARSS*, 5489–5492 (IEEE, 2021).
26. Gantayat, P., Sattar, A., Haritashya, U. K., Watson, C. S. & Kargel, J. S. Bayesian approach to estimate proglacial lake volume (BE-GLAV). *Earth Space Sci.* **11**, e2024EA003542. https://doi.org/10.1029/2024EA003542 (2024).
27. Nuth, C. & Kaab, A. Co-registration and bias corrections of satellite elevation data sets for quantifying glacier thickness change. *Cryosphere* **5** (1), 271–290 (2011).
28. Baird, T., Bristow, C. S. & Vermeesch, P. Measuring sand Dune migration rates with COSI-Corr and landsat: opportunities and challenges. *Remote Sens.* **11** (20), 2423 (2019).
29. Leprince, S., Ayoub, F., Klinger, Y. & Avouac, J. P. Co-registration of optically sensed images and correlation (COSI-Corr): An operational methodology for ground deformation measurements. In *2007 IEEE International Geoscience and Remote Sensing Symposium*, 1943–1946 (IEEE, 2007).
30. Jaboyedoff, M. et al. A review of methods used to estimate initial landslide failure surface depths and volumes. *Eng. Geol.* **267**, 105478 (2020).
31. Guzzetti, F., Ardizzone, F., Cardinali, M., Rossi, M. & Valigi, D. Landslide volumes and landslide mobilization rates in Umbria, central Italy. *Earth Planet. Sci. Lett.* **279** (3–4), 222–229 (2009).
32. Gantayat, P., Kulkarni, A. V. & Srinivasan, J. Estimation of ice thickness using surface velocities and slope: case study at Gangotri Glacier, India. *J. Glaciol.* **60** (220), 277–282 (2014).
33. Hutter, K. *Theoretical Glaciology: Material Science of Ice and the Mechanics of Glaciers and Ice Sheets*, vol. 1 (Springer, 1983).
34. Dixit, A., Sahany, S. & Mishra, S. K. Modeling the climate change impact on hydroclimate fluxes over the Beas basin using a high-resolution glacier-atmosphere-hydrology coupled setup. *J. Hydrol.* **627**, 130219 (2023).
35. Ferretti, A., Prati, C. & Rocca, F. Permanent scatterers in SAR interferometry. *IEEE Trans. Geosci. Remote Sens.* **39** (1), 8–20 (2001).
36. Perissin, D. Interferometric SAR multitemporal processing: Techniques and applications. In *Multitemporal Remote Sensing: Methods and Applications*, 145–176 (2016).
37. Hanssen, R. F. *Radar Interferometry: Data Interpretation and Error Analysis*, vol. 2 (Springer Science & Business Media, 2001).
38. Kumar, A. et al. Evolution of debris flow and moraine failure in the Gangotri glacier region, Garhwal himalaya: Hydro-geomorphological aspects. *Geomorphology*. **333**, 152–166 (2019).
39. Sattar, A. Sikkim glacial lake outburst spotlights climate vulnerability of the Himalayas. Nature India. (2023).
40. Sattar, A. et al. The Sikkim flood of October 2023: Drivers, causes, and impacts of a multihazard cascade. *Sciecne* **387**, 6740. https://doi.org/10.1126/science.ads2659 (2024).
41. Worden, C. B., Gerstenberger, M. C., Rhoades, D. A. & Wald, D.J. Probabilistic relationships between ground-motion parameters and modified Mercalli intensity in California bull. *Seism Soc. Am.* **102** (1), 204–221. https://doi.org/10.1785/0120110156 (2012).
42. Sattar, A. et al. Future glacial lake outburst flood (GLOF) hazard of the South Lhonak Lake, Sikkim Himalaya. *Geomorphology*. **388**, 107783 (2021).
43. Bhatia, N., Patel, N., Kumar, V. & others Detection and monitoring of land subsidence in Himalayan foothills using Sentinel-1 SAR interferometry. *Nat. Hazards*. **117**, 265–287. https://doi.org/10.1007/s11069-023-06046-3 (2023).
44. Khatiwada, K. R. et al. Evaluation of satellite precipitation products in the Nepal Himalaya. (2020).
45. Report, D. S. T. Sikkim, (2016). http://icestupa.org/news/slug-rb4s71, https://dstsikkim.gov.in/mech/South%20Lhonak%20Lake%20mitigation%20expedition.pdf

Acknowledgements

This work was carried out independently without the support of any funding agency or sponsors. The authors thank the SARPROZ team for providing an evaluation license for the MTInSAR processing software.

Author contributions
L.M.: Writing-original draft, visualization, validation, software, methodology, investigation, formal analysis, data curation, conceptualization. P.G.: review and editing, visualization, validation, software, methodology. A.D.: review and editing, visualization, validation, software, methodology. M.D.A.: Visualization, validation, software, methodology. R.B.: Visualization, validation, software, methodology. V.K.S.: Visualization, validation, software, methodology.

Funding

This work was carried out independently without any source of funding.

Declarations

Competing interests
The authors declare no competing interests.

Additional information
Supplementary Information The online version contains supplementary material available at https://doi.org/10.1038/s41598-026-35895-7.

Correspondence and requests for materials should be addressed to L.K.M. or P.G.